Hindawi
Advances in Materials Science and Engineering
Volume 2021, Article ID 5524591, 20 pages
https://doi.org/10.1155/2021/5524591

Research Article

Mechanism and Integrated Control of "Rib Spalling: Roof Collapse—Support Instability" Hazard Chains in Steeply Dipping Soft Coal Seams

Shuai Liu,[1,2,3] **Ke Yang**,[2,3] **and Chunan Tang**[1,4]

[1]*School of Resources and Civil Engineering, Northeastern University, Shenyang 110819, Liaoning, China*
[2]*Institute of Energy, Hefei Comprehensive National Science Center, Hefei 230031, Anhui, China*
[3]*State Key Laboratory of Mining Response and Disaster Prevention and Control in Deep Coal Mines, Anhui University of Science and Technology, Huainan 232001, Anhui, China*
[4]*School of Civil and Hydraulic Engineering, Dalian University of Technology, Dalian 116024, Liaoning, China*

Correspondence should be addressed to Ke Yang; keyang2003@163.com

Received 14 January 2021; Accepted 30 April 2021; Published 13 May 2021

Academic Editor: Robert Cerny

The hazard chain of rib spalling, roof collapse, and support instability occurring in steeply dipping coal seams (SDCSs) significantly threatens the safety and productivity of underground mining. A three-dimensional coal wall model was established considering the damage to the coal wall from the abutment pressure based on the new concept of the main control weak surface (MCWS) defined by the authors. Then, a support mechanical model under the conditions of a dynamic load induced by a sliding roof was constructed. Integrated control measurements based on the models above were developed and taken for the dangerous area of hazard chains in working faces. The results indicated that the dimensions of rib spalling were dominated by the shape, dimensions, and friction angle of the coal wall element. In detail, the order of the importance of the element failure factors, based on their sensitivities, was the roof load (6.33), the dip of the panel (−5.03), the friction angle of the coal (−3.24), the cohesion of the coal (−3.02), and the sidewall protecting force (−0.087). Additionally, the order of importance of the frictional sliding factors of the slip body was the MCWS cohesion (−0.293), roof load (0.213), and MCWS friction angle (−0.079). Equations for the threshold forces between supports under the support dumping and sliding limit states were obtained; the knowledge of these forces ensured support stability under a sliding roof. The support work resistance varied synchronously in different parts of the working face and remained within 2200–4000 kN, indicating that the proposed models and control measurements considered instrumental in hazard chain control in SDCSs were reliable.

1. Introduction

Steeply dipping coal seams (SDCSs) are coal seams with dip angles of 35–55° [1]. They are widely distributed in major coal production areas worldwide, including the Ruhr Coalfield in Germany, the Lorraine Coalfield in France, the Karaganda Coalfield in Kazakhstan, the Donbas Coalfield in Ukraine, and the West Virginia Coalfield in the US [2]. In China (Sichuan, Xinjiang, Gansu, Chongqing, and Ningxia), SDCSs have proven reserves of up to 180 to 360 billion tons and outputs of 150 to 300 million tons, accounting for 10–20% and 5–8% of all the proven reserves and outputs in China, respectively [3–5]. Due to their unique sedimentary environment, over 50% of SDCSs are coking coal and anthracite coal, which are rare varieties under protective mining [6]. SDCSs are globally regarded as complex coal seams, and mechanized mining is problematic due to the corresponding complicated rock displacement patterns and limited mining space [7]. Since the 1980s, great progress has been made in SDCS exploration due to the theoretical substantiation of fully mechanized mining, emerging mining pressure control technology, and special mining equipment development. After many years of development, SDCS mining techniques, including fully mechanized longwall,

top-coal caving mining, and stagger arrangement techniques, have been successfully applied to coal mining sites, significantly enhancing the mining efficiency [8–10]. At present, the maximum experimental mining dip angle is as high as 70°.

Since the recycling rate of the top-coal caving mining technique is quite low, the fully mechanized longwall mining of soft coal faces with large cutting heights has become a conventional technique for improving the high-efficiency recovery in thick SDCSs [11]. As the cutting height continues to rise, the stress concentration in the surrounding rock in the mined-out area gradually increases, the stress release space enlarges, and the magnitude and intensity of the surrounding rock movement grow [12]. Mining disasters such as rib spalling, roof collapse, floor heave, flying gangue, and hydraulic support instability have become more frequent in mining working faces under these conditions [13–16]. Under mining conditions of broken roofs and soft coal seams, rib spalling is usually accompanied by roof collapse, inducing fracture and moving of the immediate roof at a high level and a drastic change in the load-bearing characteristics of the support. Thus, support dumping or sliding likely occurs. These chain reaction accidents usually occur in fully mechanized mining working faces (FMWFs) of SDCSs with large cutting heights, which reduces the mining efficiency and puts the workers at the construction sites at great risk. Hence, investigating the mechanism of the "spalling roof collapse-support instability" hazard chain and proposing effective preventive or control measurements are major issues that need to be solved to ensure the safe and cost-efficient mining of SDCSs with large cutting heights.

Various theoretical studies of the mechanism of rib spalling in SDCS working faces have been reported. Zhang and Wu investigated the main patterns and characteristics of coal wall instability in steeply dipping working faces with large cutting heights and established a mechanical model for coal walls in a quarry [17]. They reported that the cutting height, false dip angle, and coal mechanical properties were closely related to the coal wall stability. Based on the spalling characteristics of the working face, Wang et al. established a vertical mechanical model for coal walls, determined the critical conditions for coal wall instability, and revealed the mining-thickness effect on coal wall stability [18]. Yang et al. utilized the plastic slip line theory to analyze the coal wall instability and determined the hazardous area of rib spalling, finding that the working face span and rotary deformation pressure of the voussoir beam on the roof were the main factors affecting rib spalling [19]. Wu et al. established a pseudoinclined working face slice element for a coal wall model using the shear failure criterion, proving that irregular tetrahedron spalling was likely to occur in the middle and upper parts of the oblique working face [20]. Wang et al. established a rock beam model for an inclined coal wall and reported that the dip angle caused the coal wall to deform asymmetrically, which explained the effect of the working face dip angle on rib spalling [21]. The above research results have significantly improved the understanding of the rib spalling mechanism in SDCS working faces.

Affected by the dip angle, the steeply dipping working face support, under the effects of the roof, floor, coal wall, coal gangue, and adjacent supports, is in an unbalanced complex stress-state environment, which makes the corresponding stability control quite challenging [22]. In recent years, numerous researchers have performed theoretical and numerical analyses of the movement trends of the surrounding rock and load-bearing characteristics of the supports in the longwall mining of SDCSs [23–26], the pushing effect between the supports and the cumulative effect [27, 28], and the coupling mechanism and instability disaster mechanism of "support-surrounding rock" [29–31]. Their findings included the support stability-instability criterion, assessment of the support critical working resistance, the enactment of anti-overturning and antiskid measures, and improvements to SDCS mining safety and efficiency.

However, these studies were mainly focused on the mechanisms of rib spalling and hydraulic support instability for SDCSs. Few of them provided in-depth analysis of the "rib spalling - roof collapse-support instability" hazard chain mechanism in soft SDCSs with large cutting heights. Moreover, to the best of our knowledge, the available mechanical models assume that the coal seam is initially intact/undamaged and disregard the plastic failure state of coal around the working face under abutment pressure [32]. In addition, the available support resistance assessments concentrated on support rotation or sliding in the critical state under stable roof conditions, while experimental studies of support dumping or sliding due to collapsed roof sliding are quite scarce.

This study's main objectives are to reveal the hazard chain mechanism in the FMWF of an SDCS with a large cutting height and to substantiate the related integrated control measurements. Considering the plastic failure state of the coal wall, a 3D model for the rib spalling of the soft coal working face was constructed, and the criteria for coal failure and sliding were proposed. In addition, the support load-bearing characteristics after spalling and roof collapse were analyzed. A mechanical model for the support stability under sliding roof conditions was proposed, making the assessment of the critical forces of the support stability under dumping and sliding conditions possible. The numerical analysis identified the areas with frequent disasters for the FMWF of an SDCS with a large cutting height under typical geological conditions. Based on the results, integrated control measurements for "spalling-roof collapse-support instability" were introduced to improve mining safety.

2. Hazard Chain in an SDCS Working Face

2.1. Basic Conditions of the Selected Working Face. The SDCS working face used as a case study is the 12124 working face of the Panbei Coal Mine in the Huainan mining area, Huainan City, Anhui Province, China (Figure 1(a)). This face featured complex geological strata groups and included two coal groups named *A* and *B* (Figure 1) located 75–90 m away from each other. The current mining was carried out only in

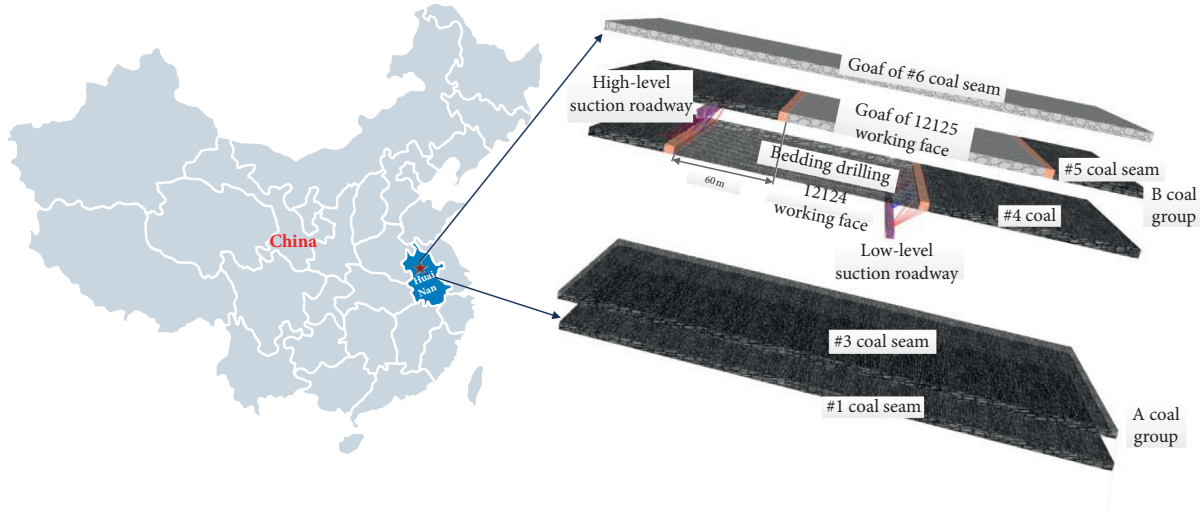

Figure 1: The 12124 working face mining conditions.

the No. 5 and No. 4 coal seams in group *B*. The typical geological conditions of the No. 4 coal seam were selected for analysis. The 12124 working face had a strike length of 1884 m and a dip width of 130 m. The strike longwall mining technique with full-seam mining for fully mechanized mining of this coal seam was adopted. The No. 4 coal seam had a thickness of 3.6–6.4 m, an elevation of the return airway of -398 m, and an elevation of the conveyance road of -478 m, while the No. 5 coal seam was approximately 20 m higher than the No. 4 coal seam, and both SDCSs had an average dip angle of 38°. Mining in the 12125 working face of the No. 5 coal seam was terminated, and a 60 m wide mining area of the 12124 working face was under the coal pillar of the 12125 working face, whereas the remaining mining area was totally under the goaf of the 12125 working face. The detailed working face geometry is shown in Figure 1.

2.2. Characteristics of Strata Behavior in the Mining Site. A ZZ7200/22/45 chock shield support was adopted in the 12124 working face, where a single-layer metal mesh, support roof beam, and face guard plate provided the support for the surrounding rock. In the early stage of mining, the "spalling-roof collapse-support instability" hazard chain (Figure 2) occurred several times with different working face severities, threatening the staff safety and equipment operation security. As shown in Figure 2, the coal wall integrity was very poor. Sometimes, the coal was in the powder form, the broken roof fell between supports, and the single-layer metal mesh was insufficient for guaranteeing safety under the support. Moreover, large-scale rib spalling usually took place in the middle-upper part of the coal wall, which implied insufficient protection by the face guard plate. Due to a steep dip angle, spalling tended to spread from the starting point in an obliquely upward direction. The spalling-induced continual roof collapse above the coal wall led to the breaking and sliding of high-level strata, overturning the support and triggering the occasional pushing between the supports.

The occurrence of the working face hazard chain during a certain period (March 5–25, 2018) was recorded and plotted in Figure 3. As observed, the hazard chain mainly occurred in the middle and upper parts of the working face dip and occurred less often in the lower part. The support work resistance, as monitored during the disasters and displayed in Figure 4, exhibited different magnitudes in various parts of the working face in the order of lower part > middle part > upper part with the respective proportions of 3 : 2:1. This nonuniform distribution in the working face resistance along the working face dip implied that the roof middle and upper parts were on the borderline between stable and unstable states, which increased the risk of overall support stability loss. The monitored working face resistance matched the hazard chain's spatiotemporal characteristics, and the real-time monitoring of the working face resistance could reflect the roof's stability conditions.

2.3. Stratigraphic Segmentation and Mechanical Properties. The occurrence of the hazard chain is closely related to the rock structure and the roof and floor physical-mechanical properties. These were obtained in field coring and laboratory tests and are depicted in Figure 5. The 12124 working face's immediate roof was an interbedded sandy mudstone compound roof with thicknesses of 6.8–7.5 m and an average thickness of 7 m. Serious argillaceous cementation within the roof and highly developed joints was observed; these issues were the main reasons why spalling caused large-scale roof collapse. The immediate floor was made of sandy mudstone with thicknesses of 1.0–3.1 m and an average thickness of 2.4 m. The average thickness of the No. 4 coal seam was 3.8 m, and the coal had a low strength. The 12124 working face was classified as a typical "three-soft" SDCS working face.

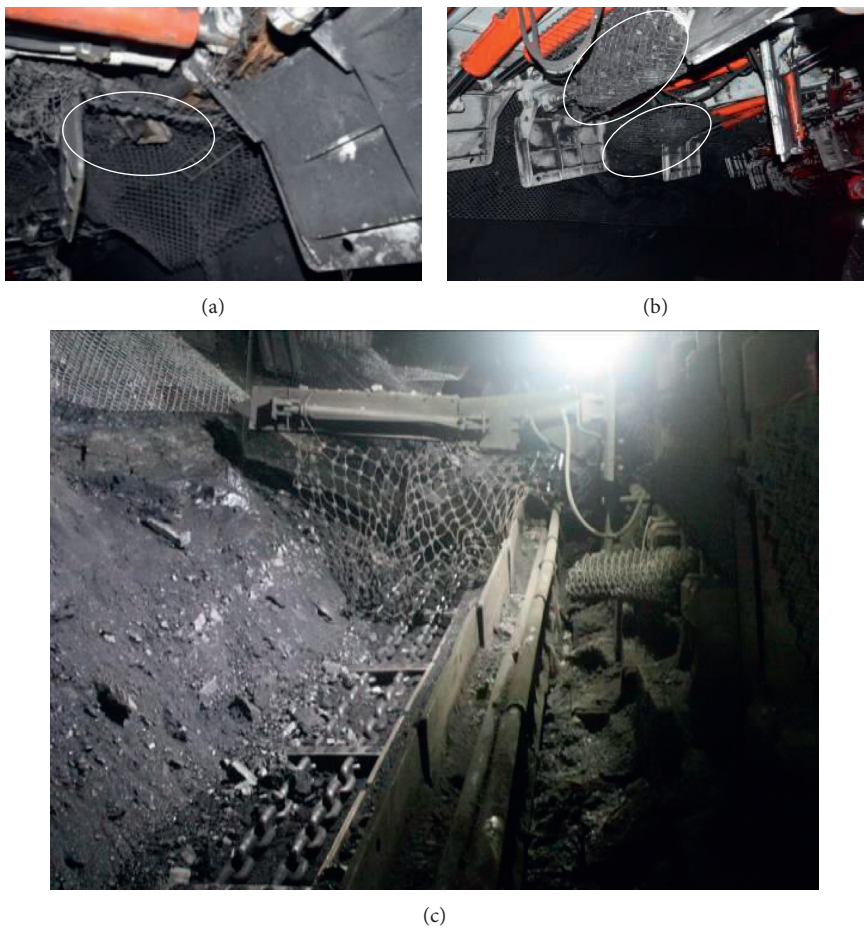

(a) (b) (c)

Figure 2: Disasters in the SDCS working face. (a) Spalling and roof collapse [15]. (b) Falling of gangues between supports [15]. (c) Spalling-caused overturning of the working face equipment.

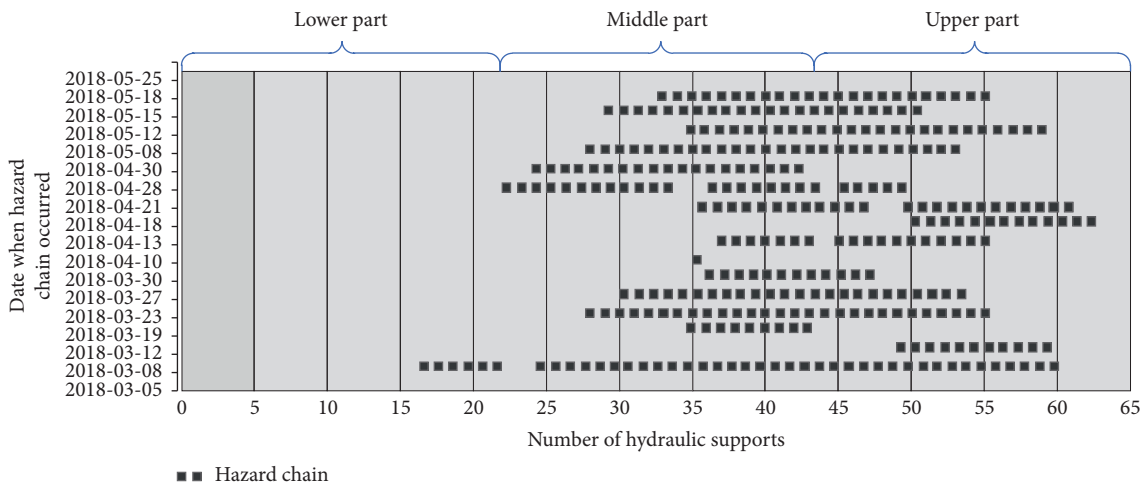

Figure 3: Recorded hazard chain occurrences in the 12124 working face.

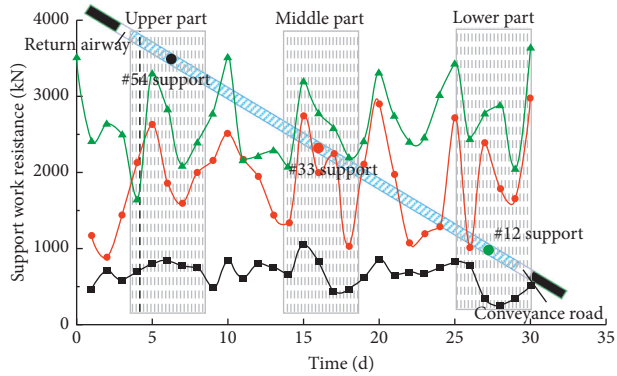

Figure 4: The support work resistance in different parts of the 12124 working face.

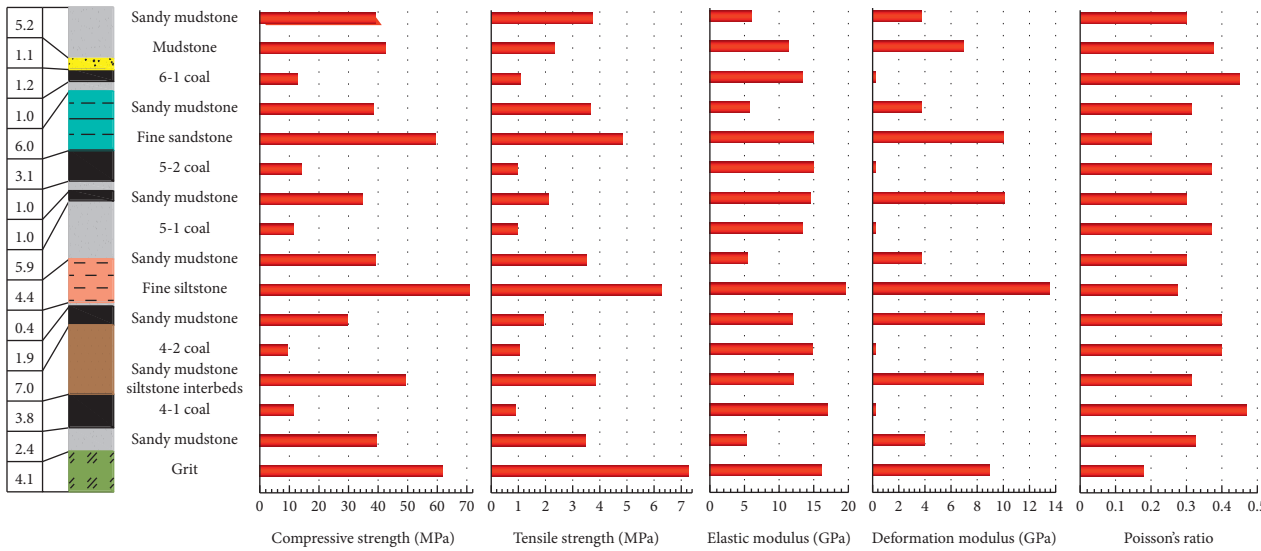

Figure 5: Physical and mechanical parameters of the roof and floor of the 12124 working face.

3. Physical and Mechanical Modeling of the Rib Spalling Process

3.1. A Physical Model of the SDCS Working Face Coal Wall. Insofar as the hazard chain in SDCS described in Section 2.2 was initiated by rib spalling, the first issue to consider is the latter's mechanism. The coal seam is naturally anisotropic and heterogeneous and initially contains numerous small joints. Under the advanced abutment pressure, the coal wall's properties begin to deteriorate as mining proceeds in the working face. A certain number of joints away from the working face continue propagating and merging, resulting in weak joint surfaces of different scales [33]. Large-scale joints can usually be seen in the coal wall at the working face, as shown in Figure 6, where the edge lines of weak joint surfaces in the coal wall are visible with the naked eye. The field monitoring results imply that macrofractures usually run through the coal seam and are parallel to the coal seam's normal line so that weak joint surfaces have the same orientation. This finding is in concert with the results reported by Wu et al. [20]. Large-scale weak joint planes can greatly reduce the coal integrity and strength. Recent studies also demonstrated that the limit equilibrium zone covered the area in front of the working face where the peak-advanced abutment pressure was reached in the coal wall and that coal in this zone was in a plastic failure state [32]. Therefore, the coal wall cannot be treated as a continuous medium, and weak joint surfaces should also be incorporated into further analysis.

When the coal strength is low, the large weak joint surfaces of the respective weak joint planes control the coal seam's mechanical behavior, classified as the main control weak surfaces (MCWSs). The latter are parallel to the normal coal seam line and cut off the coal near the working face into elements with a weak mechanical adhesion with the surrounding coal. The coal wall stability depends on the mechanical properties and stress-strain state of the element. Recent studies proved that soft coal seams' rib spalling is a shear failure of coal under roof pressure [34]. When the coal has low strength, the elements exhibit shear failure and become slip bodies under roof pressure and coal self-weight. Spalling is induced when the surrounding elements and support are insufficient for inhibiting the sliding elements along the MCWS. Since the MCWS is randomly distributed,

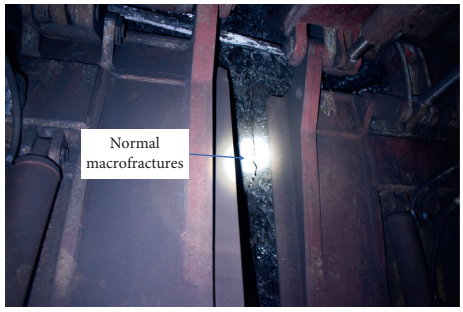

Figure 6: Normal macrofractures in the working face.

the shapes of the different elements vary a lot greatly. A triangular prism model (Figure 7) represents the element adjacent to the coal wall face related to the MCWS.

Based on the above concept, a physical-mechanical coal wall model of the soft SDCS with a large cutting height was developed, as shown in Figure 7. Herein, P is the normal load transferred from the roof to the coal wall, and α is the dip angle. Under the advanced abutment pressure, the primary joints developed into MCWS $abc\ d$ and $bfec$ planes that formed a triangular $abf\ dc\ e$ prism with weak mechanical adhesion with the surrounding coal. The Mohr–Coulomb criterion was used to analyze the triangular prism elements of any random shape, which yielded the respective conditions/criteria of the shear failure and the frictional sliding of the slip body. Although the actual shear slip surface is usually curved, the limited heights of the coal seam and spalling made it possible to treat the fractured surface $a'bf'$ in Figure 7 as a plane to simplify the analysis. The specific descriptions and details of this model have been presented and published in reference [13], so this paper gives only a brief presentation.

3.2. Mechanical Criterion for the Shear Failure of the Soft Coal Wall Element. The triangular prism $abf\ dc\ e$ undergoes shear failure along the MCWS $abc\ d$ and MCWS $bfec$ planes due to the roof pressure, gravity, sidewall protecting force, and surrounding element confining pressure. Shear fracture traces ba' and bf' are formed, and the surface $ba'f'$ formed by the intersection of the two traces is the fracture surface of the element. According to the Mohr–Coulomb criterion, the shear failure criterion of MCWS $bfec$ and MCWS $abc\ d$ can be formulated as the difference in the slip force F along the shear plane and the shear resistance D along the same plane. Shear failure takes place when the difference is larger than zero, which is

$$W = F - D \geq 0 \tag{1}$$

Figure 8 is the diagram of the shear failure of the two MCWSs. Here, θ is the angle between the shear plane and coal wall, q is the roof load, N is the normal force on the shear plane, P_h is the sidewall protecting force provided by the hydraulic support, G is the gravity of the coal wall slip body, G' is the component of G on MCWS $bfec$, G'' is the component of G on MCWS $abc\ d$, h_1 is the cracking height of MCWS $bfec$, h_2 is the cracking height of MCWS $abc\ d$, and ζ and κ are the angles between the component of G on the MCWS $bfec$ and MCWS $abc\ d$ and the coal wall. From the spatial geometric relationship in Figure 8, we can obtain $\omega = \theta - \zeta$ and $\psi = \theta + \kappa$.

When both W_1 and W_2 exceed zero, the triangular prism $abf\ dc\ e$ undergoes shear failure along the surface $ba'f'$ to form a slip body. A series of derivations result in the criterion for the shear failure of the weak coal wall element with the consideration of the confining pressure:

$$\begin{cases} qh_1 \cot\theta(\sin\theta - \cos\theta\tan\varphi) - Ch_1\csc\theta + G\sqrt{1-\sin\alpha^2\cos\beta^2} \\ \times\left(\dfrac{\sin\theta - \cos\theta\sin\beta\tan\alpha}{\sqrt{1+\sin^2\beta\tan^2\alpha}} - \dfrac{\cos\theta + \sin\theta\sin\beta\tan\alpha}{\sqrt{1+\sin^2\beta\tan^2\alpha}}\tan\varphi\right) - P_h(\cos\theta + \sin\theta\tan\varphi) \geq 0, \\ qh_2 \cot\theta(\sin\theta - \cos\theta\tan\varphi) - Ch_2\csc\theta + G\sqrt{1-\sin\alpha^2\cos\gamma^2} \\ \times\left(\dfrac{\sin\theta + \cos\theta\sin\gamma\tan\alpha}{\sqrt{1+\sin^2\gamma\tan^2\alpha}} - \dfrac{\cos\theta - \sin\theta\sin\gamma\tan\alpha}{\sqrt{1+\sin^2\gamma\tan^2\alpha}}\tan\varphi\right) - P_h(\cos\theta + \sin\theta\tan\varphi) \geq 0, \end{cases} \tag{2}$$

where β and γ are the angles between MCWS $bfec$ and MCWS $abc\ d$ and the coal seam strike, respectively, and are random, C is the cohesion of the coal, and φ is the internal friction angle.

3.3. Sliding Criterion of the Slip Body. Once a slip body is formed after triangular prism shear failure, it slips along the fracture plane $ba'f'$ as the rib spalls when the support from the MCWS and side guard is insufficient. Rib spalling usually

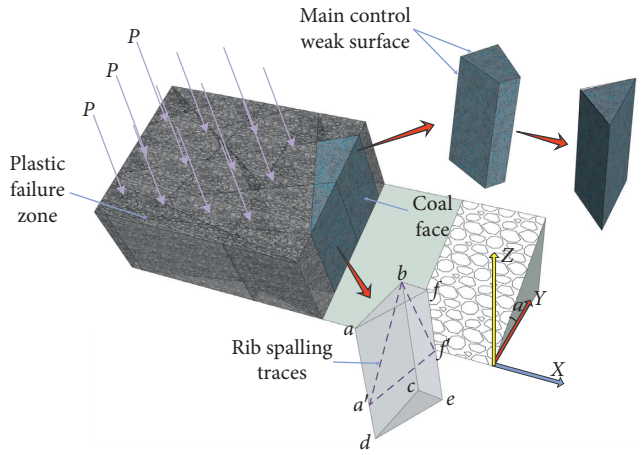

Figure 7: Physical-mechanical model of the coal wall.

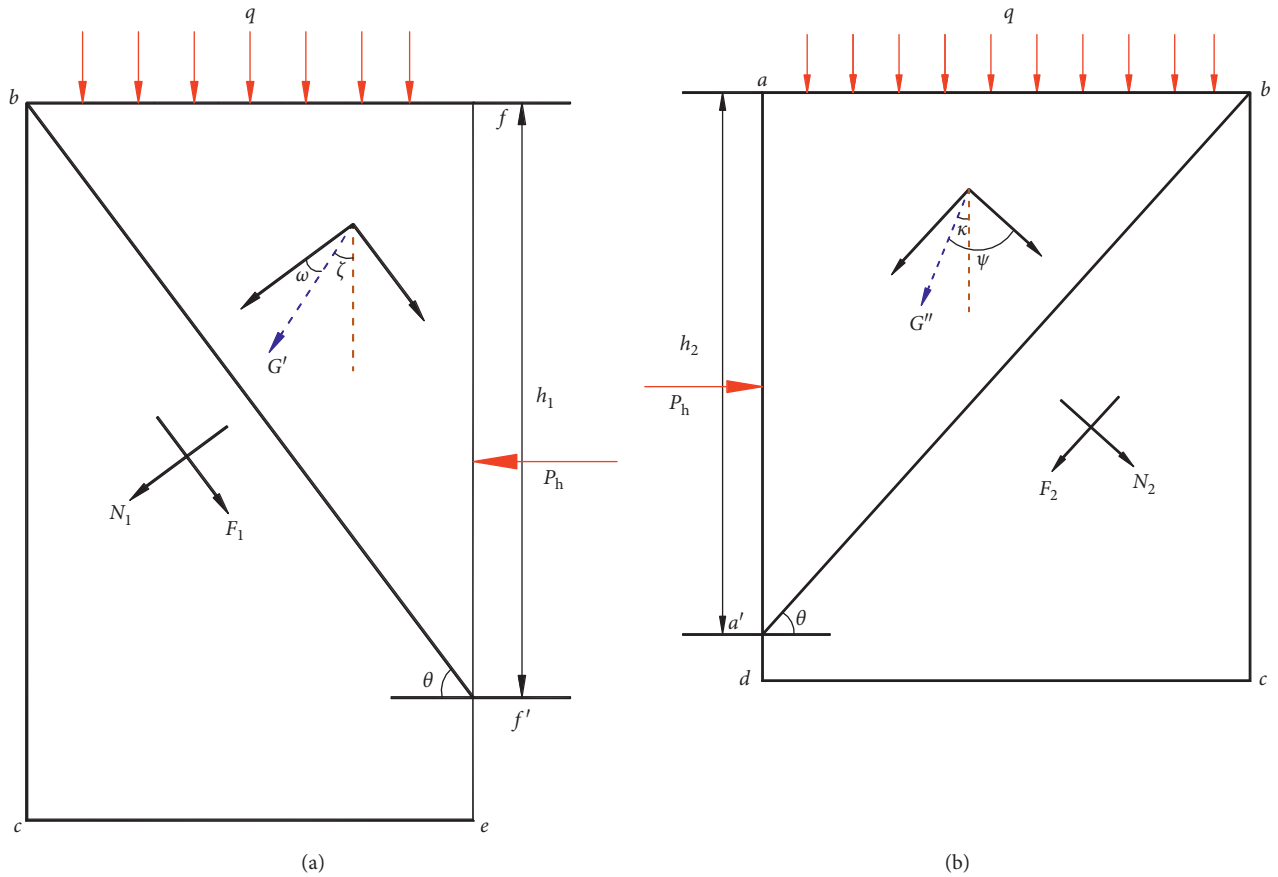

Figure 8: Analysis of shear failure of MCWS. (a) MCWS *bfec*; (b) MCWS *abcd*.

occurs during the period of coal cutting and support removal, so the effect of the sidewall protecting force on the slip body is not considered.

The stability coefficient K of the slip body is expressed as

$$K = \frac{\left(P_1 \sin\theta + G' \sin\omega + P_2 \sin\theta + G'' \sin\psi\right)}{\left(\mu_s\left(P_1 + G'\cos\zeta\right)v/(1-v) + 1/2C_s h_1^2 \cot\theta + \mu_s\left(P_2 + G''\cos\kappa\right)v/(1-v) + 1/2C_s h_2^2 \cot\theta\right)}, \quad (3)$$

where μ_s is the sliding coefficient of the MCWS, C_s is the MCWS cohesion, and v is coal's Poisson's ratio.

At $K > 1$, the slip body causes frictional sliding. At $K \leq 1$, even if the element has been broken, there is no sliding instability, and no rib spalling occurs in the coal wall.

3.4. Rib Spalling Mechanism of the SDCS Working Face

3.4.1. Location and Scale of Rib Spalling. The proposed physical-mechanical model demonstrated that the soft element's failure started at the top point b and that the shear line extended to the coal wall with an angle θ ($\theta = \pi/4 + \varphi/2$). A slip body was formed in the middle-upper part of the coal wall, which matched the field monitoring data. Notably, Yin et al. also reported that the most likely location of soft coal wall instability was the middle-upper part (at 65% of the cutting height) [35]. Moreover, Ning revealed that the coal wall experienced a small deflection under mining-induced stress and then continued deforming until it reached its peak deflection when fracturing occurred at a distance from the coal wall top corresponding to 35% of the cutting height [36]. The results of this study are consistent with previous research results. It was also found that, as the rupture line extended along the angle θ towards the coal wall, the rib spalling scales in the same working face were controlled by the shape, size, and friction angle of the above element.

3.4.2. Shear Failure Mechanism of the Coal Wall Element. The above theoretical analysis showed that failure occurred in weak elements if the shear failure conditions were satisfied in both MCWSs. It follows from equation (2) that when the spatial shape of the element is determined, parameters G, h_1, h_2, β, γ, and θ are constant. Therefore, shear failure in the element is mainly related to the roof load q, coal cohesion C, internal friction angle φ, coal seam inclination α, and sidewall protecting force P_h. Based on the above analysis and spatial shape of the triangular prism of the 12124 working face, single-factor analysis was carried out to reveal the dominant influencing parameters leading to the failure of the coal wall element. The initial geometrical, physical, and mechanical parameters of the triangular prism were chosen as follows: β and γ were 30° and 60°, respectively, the vertical distance between point b and the coal wall was 1.5 m, and the internal friction angle $\varphi = 20°$; thus, $\theta = 55°$; $h_1 = 2.47$ m, $h_2 = 4.28$ m, the coal cohesion $C = 3$ MPa, the coal seam inclination $\alpha = 38°$, the roof load $q = 9$ MPa, the sidewall protecting force $P_h = 0.2$ MPa, and Poisson's ratio of coal $v = 0.45$.

The calculation of the point elastic coefficient of a function is the common technique used in single-factor sensitivity analysis. The change in the dependent variable due to an independent variable can be obtained. However, this method applies to only small changes in the independent variable. Due to the large changes in each factor considered in this study and the point elastic coefficients between different values in one factor, sensitivity analysis is not suitable here. However, regarding this method, this study defined the sensitivity as the ratio of the difference in the dependent variable to the rate of change in the independent variable. The mathematical meaning is the change in the dependent variable when the change in the independent variable reaches 1%. Thus, the larger the change in the dependent variable is, the more sensitive the factor is.

The roof load q in equation (2) versus the difference W in the sliding force F and shear resistance D with the two MCWSs as the dependent variable is plotted in Figure 9(a). Since the coal wall was in the plastic failure zone (i.e., the unloading zone), the roof load was in the range of 6–11 MPa. As seen in Figure 9(a), the W values of MCWS $bfec$ and MCWS $abc\ d$ linearly increased with the load, indicating that the triangular prism element experienced decreasing stability under increasing roof load. The variable's minimum value was equal to unity, and the other variables were the multiples of the real values to the minimum value. Since the sensitivities of the linear functions describing the stable state of MCWS $bfec$ and MCWS $abc\ d$ were 6.33 and 10.98, respectively, the stability of MCWS $abc\ d$ was more sensitive to roof load variation. This was because the coefficient of the roof load q was related to the cracking height h. In addition, the condition $W \geq 0$ was first satisfied when the load reached 8.65 MPa, and shear failure first took place in MCWS *abcd*, and MCWS $bfec$ experienced failure as the roof load further increased to 8.74 MPa. Therefore, MCWS $bfec$, with a sensitivity of 6.33, required a higher roof load for failure, which was critical for the element stability, reflecting the impact of the roof load q on the stability of the triangular prism element.

Figure 9(b) illustrates the effect of the cohesion C on W. The cohesion of coal was selected as 1–10 MPa. As seen in Figure 9(b), the values of W of MCWS $bfec$ and MCWS $abc\ d$ linearly decreased with the cohesion C. The function monotonically decreased, suggesting that the element stability improved with the cohesion. Since the sensitivities of the linear functions describing the stable state of MCWS $bfec$ and MCWS *abcd* were -3.02 and -5.22, respectively, the stability of MCWS *abcd* was more sensitive to changes in the cohesion. This was because the coefficient of cohesion depended on the cracking height h and $h_2 > h_1$. It can be seen that $W \geq 0$ first occurred when the cohesion decreased to 3.02 MPa, and shear failure first took place in MCWS $abc\ d$. Therefore, MCWS $bfec$, with a sensitivity of -3.02, was critical to the stability of the element, reflecting the impact of the cohesion C on the triangular prism element's stability.

The influence of the friction φ on W is illustrated in Figure 9(c). The friction angle of coal was selected as 16–40°. As seen in Figure 9(c), the W values of MCWS $bfec$ and MCWS $abc\ d$ linearly decreased with the friction angle φ. The function monotonically decreased, suggesting that the stability of the element improved as the friction angle increased. Since the sensitivities of the linear functions describing the stable state of MCWS $bfec$ and MCWS *abcd* were -3.24 and -5.57, respectively, the stability of MCWS *abcd* was more sensitive to changes in the friction angle. In addition, $W \geq 0$ first occurred when the friction angle dropped to 20.3°, and shear failure first took place in MCWS *abcd*, while MCWS $bfec$ experienced failure when the friction angle decreased to 19.8°. Therefore, MCWS $bfec$,

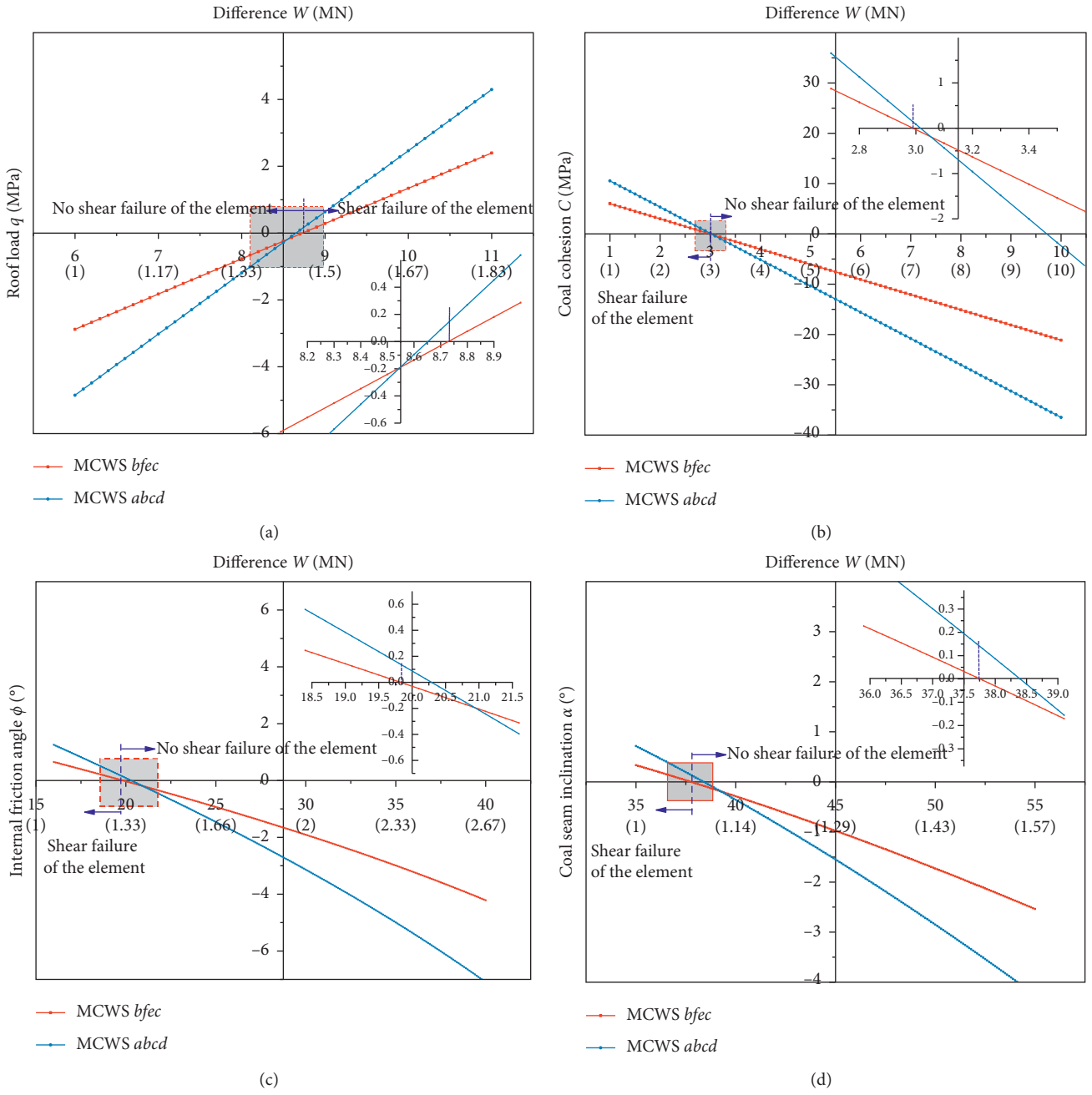

Figure 9: Continued.

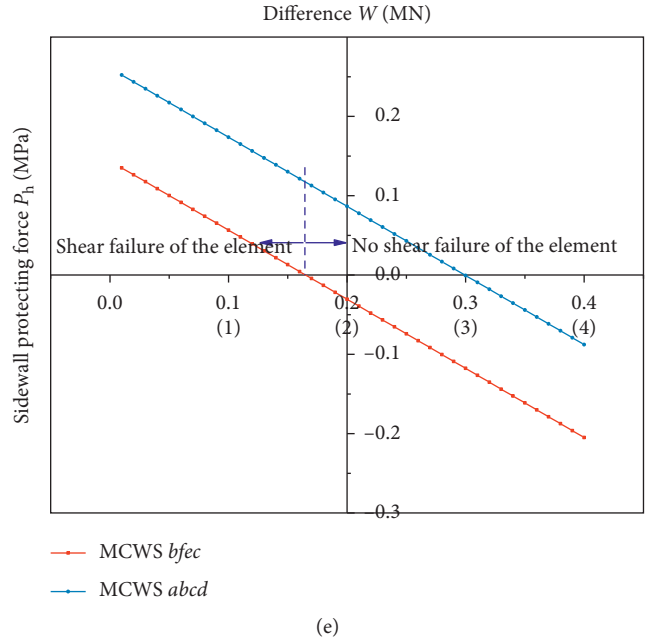

FIGURE 9: The impacts of the main factors on the shear failure of the element. (a) The impact of the roof load q on W. (b) The impact of the cohesion C on W. (c) The impact of on W. (d) The impact of α on W. (e) The impact of the sidewall protecting force P_h on W.

with a sensitivity of −3.24, was critical to the stability of the element, reflecting the impact of the friction angle φ on the stability of the triangular prism element.

Figure 9(d) depicts the effect of the coal dip angle α on W. The coal dip range was selected as 35–55° to consider SDCSs. As seen in Figure 9(d), the W values of MCWS $bfec$ and MCWS $abcd$ linearly decreased as the coal dip α increased. The function monotonically decreased, suggesting that the stability of the element improved as the coal dip increased. Since the sensitivities of the linear functions describing the stable states of MCWS $bfec$ and MCWS C were −5.03 and −8.69, respectively, the stability of MCWS $abc\ d$ was more sensitive to the change in coal dip. It could also be seen that $W \geq 0$ first occurred when the coal dip decreased to 38.38°, and shear failure first took place in MCWS $abcd$, while MCWS $bfec$ experienced failure when the coal dip dropped to 37.75°. Therefore, MCWS $bfec$, with a sensitivity of −5.03, was critical to the stability of the element, reflecting the impact of the coal dip φ on the triangular prism element stability.

Figure 9(e) illustrates the influence of the sidewall protecting force P_h on W. The sidewall protecting force was selected as 0–0.4 MPa. As seen in Figure 9(e), the W values of MCWS $bfec$ and MCWS $abcd$ linearly decreased as the sidewall protecting force P_h increased. The function monotonically decreased, suggesting that the stability of the element improved as the sidewall protecting force increased. The linear functions describing the stable states of MCWS $bfec$ and MCWS $abcd$ were parallel and had the same sensitivity of -0.087. It was found that $W \geq 0$ first occurred as soon as the sidewall protecting force reached 0.3 MPa. At this moment, shear failure first took place in MCWS $abcd$, while MCWS $bfec$ experienced failure when the sidewall protecting force P_h reached 0.165 MPa. Therefore, MCWS $bfec$, with a sensitivity of −5.03, was critical to the stability of the element, reflecting the impact of the sidewall protecting force P_h on the stability of the triangular prism element.

The above analysis revealed the following order for the sensitivities of all the factors controlling the shear failure of the coal wall: roof load q (6.33), coal dip α (−5.03), friction angle of the coal φ (−3.24), cohesion of the coal C (−3.02), and sidewall protecting force P_h (−0.087). The minus sign implies that the W value decreases, while the coal wall stability increases as the independent variable increases. Hence, reducing the roof load and increasing the working face dip are two major approaches for preventing the coal wall from shearing. However, increasing the working face dip can significantly increase the risk of the falling and sliding of the support and mining equipment. Thus, only the cohesion and friction angle should be increased to achieve this goal. Increasing the sidewall protecting force can also prevent the coal wall elements from shearing. Nevertheless, the increment in the force from the equipment is limited, as is the element strength increment. Wang [34] and Tai et al. [37] proposed a plane strain model of coal wall carving and reported that both tensile and shear failures were related to the roof pressure, shear strength, and characteristics of the coal. Therefore, decreasing the pressure on the coal wall and increasing the shear strength and cohesion of the coal were the main methods for preventing the coal wall from spalling.

However, no sensitivity or coal dip analyses were conducted in [34, 37], while the findings in this study are corroborated by the above analyses.

3.4.3. Frictional Sliding Mechanism of the Slip Body. The proposed mechanical model revealed that spalling occurred only when element failure and sliding occurred simultaneously. Although most researchers believe that spalling induces coal wall failure, we believe that coal failure causes a sliding body that can remain in a stable state as long as the clamping from the MCWS can resist the roof load and self-weight of the slip body. The sliding criterion of the slip body via equation (3) implies that once a slip body is formed, the stability coefficient K is controlled by the roof load q, MCWS friction angle φ_s ($\mu_s = \tan \varphi_s$), and MCWS cohesion C_s. Sensitivity analysis of frictional sliding, based on equation (3) and discussed in Section 3.4.2, was conducted in this study.

Figure 10(a) describes the function where the roof load q in equation (3) is the independent variable and the stability coefficient K is the dependent variable. Since the element bearing capacity continually decreased after the failure of the element, the roof load dropped to 1–8 MPa. Figure 10(a) shows that K linearly increased as q increased, indicating the possibility of frictional sliding of the slip body increasing with the roof load. As the roof load q increased to 3.9 MPa, $K > 1$ and the stable state of the slip body shifted to a frictional sliding state. Figure 10(a) displays that the function's sensitivity describing the sliding state of the slip body is 0.213, which reflects the effect of the roof load q on the frictional sliding of the slip body.

Figure 10(b) plots the friction angle φ_s of the MCWS as an independent variable versus the stability coefficient K as the dependent variable. The chosen friction angle was in the range of 7–30°. Figure 10(b) shows that K linearly increased as φ_s decreased, indicating the possibility of reduced frictional sliding of the slip body as the friction angle φ_s increased. As the friction angle φ_s increased to 17.7°, the condition $K > 1$ was satisfied, and the slip body's frictional sliding state shifted to a stable state. Figure 10(b) shows that the sensitivity of the function describing the sliding state of the slip body is −0.079, which reflects the impact of the friction angle φ_s on the frictional sliding of the slip body.

The function, which implies that the cohesion C_s of MCWS in equation (3) is the independent variable and that the stability coefficient K is the dependent variable, is plotted in Figure 10(c). Since the cohesion of the MCWS was remarkably lower than that of coal, the cohesion value range was preset at 0.5–5 MPa. As seen in Figure 10(c), K decreased as the cohesion increased, indicating the possibility of reduced frictional sliding of the slip body with the cohesion C_s. As the latter increased to 1.6 MPa, the condition $K > 1$ was satisfied, and the slip body shifted from a frictional sliding state to a stable one. It was also found that the absolute slope of the function dramatically decreased as the dependent variable increased. Thus, changes in the cohesion C_s had a significant effect on the slip body shift to a stable state from a frictional sliding state. For the convenience of comparison, the function was regarded as linear during the sensitivity analysis, which led to a sensitivity of -0.293. This sensitivity reflected the effect of the cohesion C_s of the MCWS on the frictional sliding of the slip body.

The sensitivity analysis made it possible to rank the sensitivities of all the factors in the following order: MCWS cohesion C_s (−0.293), roof load q (0.213), and MCWS friction angle φ_s (−0.079). The minus sign implies that the K value decreased, and the stability of the coal wall increased as the independent variable increased. Hence, increasing the MCWS cohesion and reducing the roof load were important steps for preventing the coal wall from frictional sliding. However, increasing the friction angle of the MCWS provided a very limited improvement in the slip body stability.

4. Variation in the Support Load Bearing Characteristics Induced by the Spalling - Roof Collapse Hazard Chain

During strike longwall mining in SDCSs, the working face roof behavior is a key factor controlling the support stability. Luo et al. investigated working face roof deformation, failure, migration, and spatial structure formation. They reported the temporal sequence and asymmetry in the dip direction, as well as their variations in different parts of the strike [22]. Our field monitoring data demonstrated that due to the influence of the dip angle, the distance between the caving gangue and support gradually increased from the bottom to the top along the working face [11]. This implies that the mined-out area is under a nonuniform filling state along the working face dip due to a steep dip angle since a nonzero angle β is formed by the floor/support and caving gangue/floor contact lines. Notably, these two contact lines are usually parallel to each other in coal seams with common dip angles, as shown in Figure 11. The bottom area in the dip of the mined-out area is densely filled, space for roof movement is limited, and the "support-surrounding rock" system is stable. The middle-upper part is not filled or the filling gangue is far from the working face. The magnitude and intensity of the roof movement are large, and the surrounding rock in the working face has poor stability. Since the roof pressure is borne by the support system made of coal in front of the coal wall, support, and caving gangue, the support and coal wall in the middle-upper part of the working face bear a large portion of pressure. This is why rib spalling tends to occur in this area and why the spatial roof structure is asymmetric.

When rib spalling occurs in the working face of soft SDCSs, the free space for the soft crashed roof in front of the support beam to fall is extended, which causes the roof above the support continue to fall and spread upward like a fan, making the support under no-load conditions evident, as shown in Figure 11. Then, the enlarged roof space causes the immediate roof above the upper adjacent supports to spall and slide down to the upper part of the bottom supports, changing their load-bearing characteristics. Since the roof above the supports shifts to a sliding state from a stable one, the difficulty of support stability control is increased

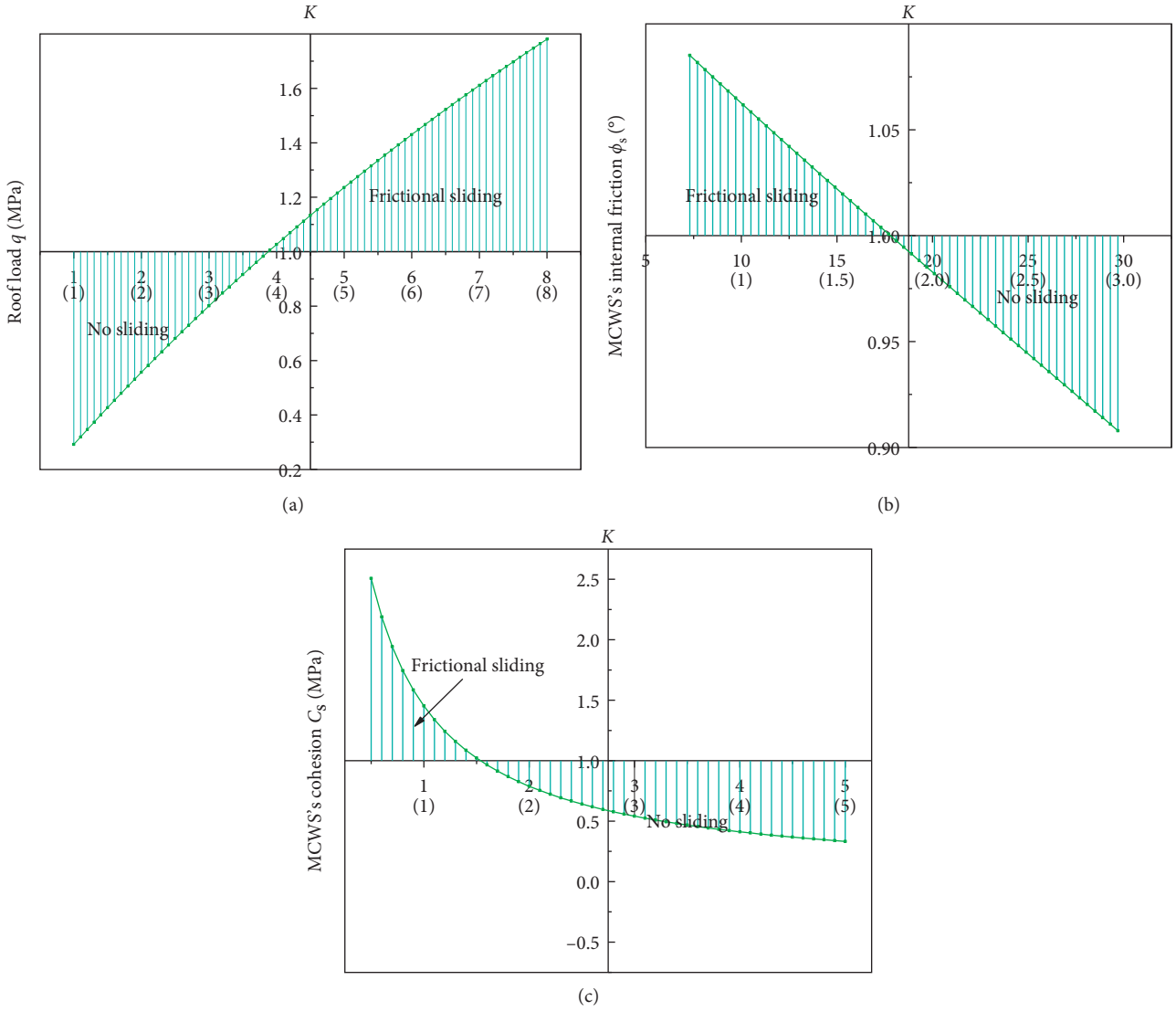

Figure 10: The impact of the main factors on frictional sliding of the slip body. (a) The impact of roof load q on K. (b) The impact of the MCWS friction angle φ_s on K. (c) The impact of MCWS's cohesion C_s on K.

(Figure 12). Additionally, when several adjacent supports are under no-load conditions, the roof pressure transfers to the deep part of the coal wall, leading to large-scale spalling and causing a vicious cycle of "spalling-roof collapse-support instability-large-scale spalling."

5. Mechanical Analysis of the Support Stability

The available mechanical models [37–39] do not apply once the support's load-bearing characteristics are changed. A single support was selected for analysis to facilitate this study, and its loading conditions are depicted in Figure 13.

The stability of the hydraulic support is controlled by the strike and dip of the coal seam. In 3D space, the support gravity G_s is decomposed into the components G_2 (parallel to the normal vector of coal, which is positive to the stability of support) and G_1 (parallel to the dip direction, which increases the tendency of support dumping and sliding).

It follows from Figure 13 that

$$G_2 = G_s \cos \alpha \cos \varpi, \tag{4}$$

where G_s is the support gravity, kN, α is the dip angle, °, and ϖ is the downward mining angle, °.

The force G_1 is parallel to the dip direction and support roof and normal to G_2. Hence, G_1 is expressed as

$$G_1 = G_s \sqrt{1 - (\cos \alpha \cos \varpi)^2}. \tag{5}$$

Ignoring the effect of the advancing jack on the support, a mechanical model along the dip was built, as shown in Figure 14.

Herein, the positive direction is a reverse rotation of the support; h is the cutting height, m; B is the base width of the support, m; F_c' is the normal load from the sliding roof acting on the support, kN; f_2 is the friction between the support and the sliding roof, kN; x_0 is the point of application of the

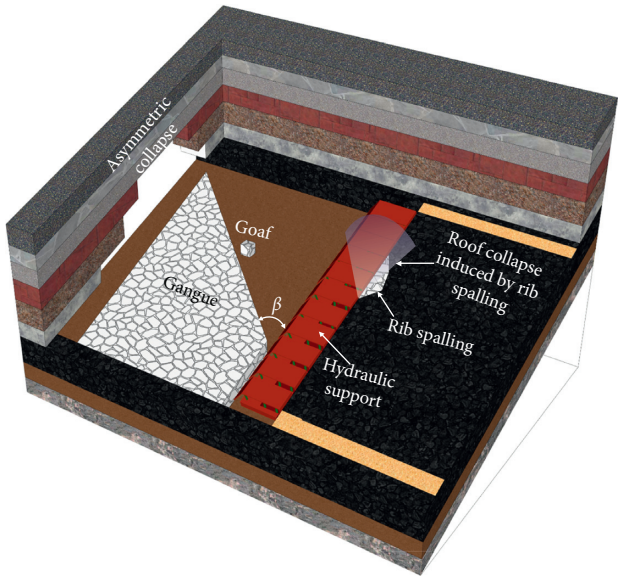

Figure 11: Filling characteristics of the mined-out area and instability forms of the surrounding rock in the working face.

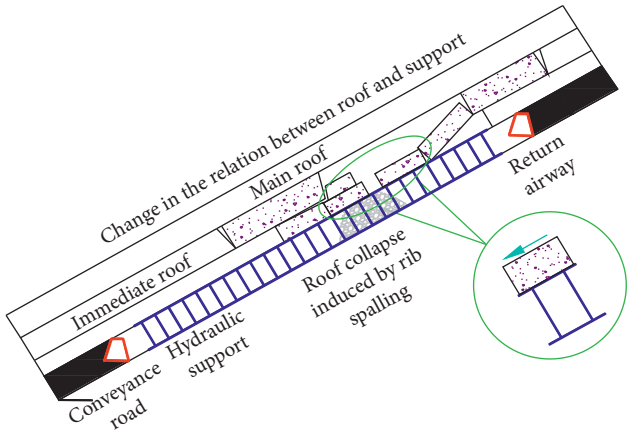

Figure 12: Change in the relation between the immediate roof and support caused by spalling roof collapse.

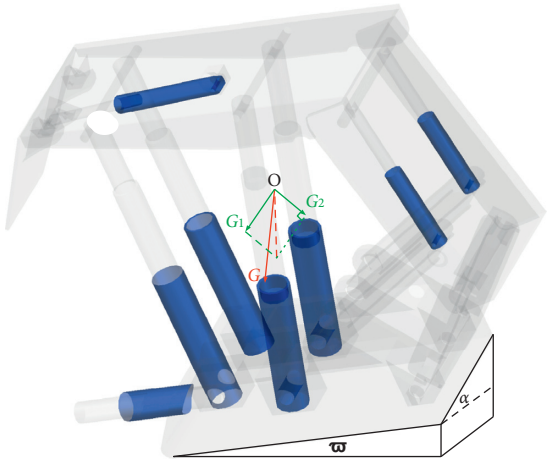

Figure 13: Loading condition of the support, with its self-weight.

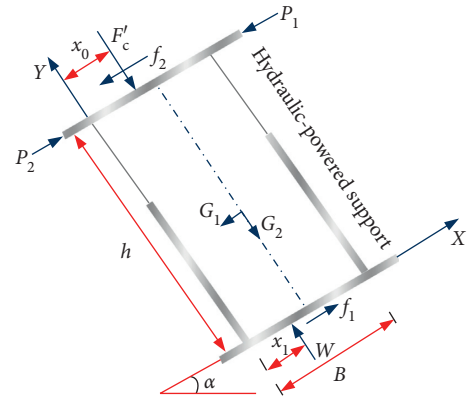

Figure 14: Mechanical model of the hydraulic-powered support.

normal load from the sliding roof, m; W is the normal load from the floor acting on the support, kN; f_1 is the friction between support and floor, kN; x_1 is the point of application of the normal load from the floor, m; P_1 and P_2 are the loads from the adjacent supports; and, μ_1' and μ_2' are the roof/support and floor/support friction coefficients, respectively.

The sliding roof pressure F_c that acts on the support is expressed as

$$F_c = \chi H L_s B, \tag{6}$$

where χ is the body force, kN/m^3, H is the immediate roof thickness, m, and L_s is the support length, m.

During mining, when the point of application $x_0 = B$ of the normal load F_c' from the sliding roof and the normal load W from the floor, which jointly acts on the support, is shifted to $x_1 = 0$, the support experiences a critical ultimate dumping limit state. According to the moment equilibrium condition, the following equations were derived:

$$\begin{cases} hf_2 + \dfrac{h}{2}G_1 - h(P_2 - P_1) - BF_c' - \dfrac{B}{2}G_2 = 0, \\ F_c' = F_c \cos\alpha, \\ f_2 = \mu_2' F_c \cos\alpha. \end{cases} \tag{7}$$

Substituting equations (4)–(6) into equation (7) gives the critical forces between supports provided by the side guard plate under the ultimate dumping limit state:

$$\begin{aligned} P_f = P_2 - P_1 &= \left(\mu_2' - \frac{B}{h}\right)\chi H L_s B \cos\alpha \\ &+ \frac{G_s}{2}\left(\sqrt{1 - (\cos\alpha\cos\varpi)^2} - \frac{B}{h}\cos\alpha\cos\varpi\right). \end{aligned} \tag{8}$$

When the point of application of the normal load F_c' becomes $x_0 = B/2$ and the normal load W is shifted to $x_1 = B/2$, the support tends to slide under the action of forces of F_c and G_s. The following equations describe the support in the critical sliding state:

$$\begin{cases} (P_2 - P_1) + f_1 - G_1 - f_2 = 0, \\ W - F_c' - G_2 = 0, \\ f_1 = \mu_1' W. \end{cases} \tag{9}$$

The substitution of equations (4)–(6) into equation (9) yields the critical force between the support provided by the side guard plate in the critical sliding state:

$$P_s = P_2 - P_1 = (\mu_2' - \mu_1')\chi H L_s B \cos\alpha - G_s \mu_1' \cos\alpha \cos\varpi + G_s \sqrt{1 - (\cos\alpha \cos\varpi)^2}. \tag{10}$$

6. Engineering Applications

6.1. Areas with a High Risk of Hazard Chain Occurrence. The hazard chain event starts with rib spalling, and it can be seen from equations (2) and (3) that when the coal endowment in the working face of a soft SDCS with a large cutting height is determined, the roof pressure is the key factor controlling the spalling occurrence in the coal wall. Given the 12124 working face's complex mining conditions, the roof pressure distribution in the working face should be analyzed first to identify the areas with a high risk of hazard chain occurrence.

The middle-upper part of the 12124 working face is located below the upper coal pillars of the 12125 working face area. During mining, the roof's load-bearing characteristics in the 12124 working face may be influenced by the adjacent coal pillars. A numerical model for mining the 12124 working face, as shown in Figure 15, was established with FLAC3D based on the mining site's conditions. The model is 200 m wide, 270 m high, and 400 m long. To clearly show the details of the dip section, a strike length of only 100 m is intercepted for display. The Mohr–Coulomb criterion was used to describe the constitutive relation. Vertical and horizontal displacement constraints were applied to the model bottom and periphery, respectively, whereas the stress boundary condition was applied to the model top. Mining in the 12125 working face in the No. 5 coal seam was followed by mining in the 12124 working face in the No. 4 coal seam when stress field equilibrium in the 12125 working face was achieved.

When the 12125 working face mining was completed, the stress field in the surrounding rock and No. 4 coal seam below it was obtained, as shown in Figure 16. As observed, a distressed zone was formed in the No. 4 coal seam below the mined-out area of the 12125 working face, where the initial stress of 11–13 MPa was reduced to 6 MPa. A stress concentration was induced under the side coal pillars in the mined-out area with the stress peak values of 18 and 20 MPa in the lower and upper parts, respectively. A mining area with a width of 60 m in the 12124 working face was laid out below the coal pillar in the return airway of the 12125 working face, and the vertical stress in this area grew to 14–18 MPa from 10–12 MPa. Thus, the No. 4 coal seam's initial stress state was disturbed by mining in the 12125 working face.

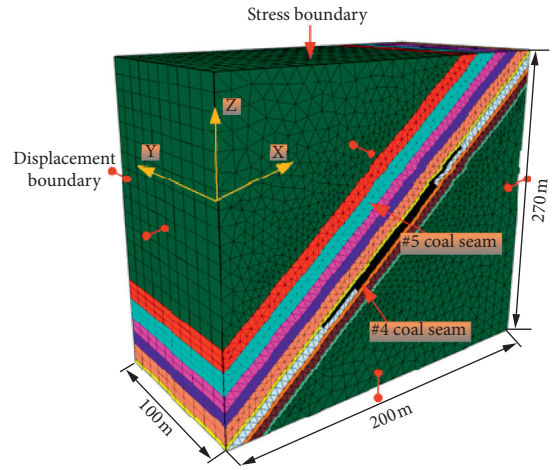

Figure 15: The numerical model of the geological conditions of the 12124 working face.

When stress equilibrium was achieved, mining was started in the 12124 working face of No. 4. Figure 17 depicts the distribution of the abutment pressure in front of the working face during mining. Due to the advanced abutment pressure, the vertical stress in the coal wall of working face 12124 was much higher than that before mining, namely, to 12–16 MPa from 6 MPa under the mined-out area. Additionally, the vertical stress in the coal wall below the pillar increased to 28–34 MPa from 14–18 MPa, showing a twofold increment. The vertical stress in the coal wall in a 60 m-wide working face below the pillar was 2.1–2.3 times higher than that under the mined-out area, and this parameter increased gradually from the return airway, peaking at 46 m. This demonstrated that this area had a high risk of hazard chain occurrence, which was consistent with the available disaster records of the mining sites.

6.2. Integrated Control Measurements. Based on the revealed forms of hazard chains in the 12124 working face and the corresponding mechanisms, as well as numerical simulation results and mining practice, this study proposed the following integrated support measures preventing rib spalling, roof collapse, and support instability:

(1) The 60 m-wide middle-upper part in the dip of the 12124 working face is a high-stress concentration zone, classified as an area with a high risk of hazard chain occurrence; the proposed integrated control measurements should be applied to this particular region.

(2) The work resistance of the hydraulic support should be increased by one-third of its original value. Since the roof load represents the first- and second-most influential parameter on the shear failure and the sliding of the slip body, respectively, the main function of the hydraulic support is to support the roof jointly with the coal wall, to resist pressure, to considerably increase the work resistance, and to reduce the pressure borne by the coal wall.

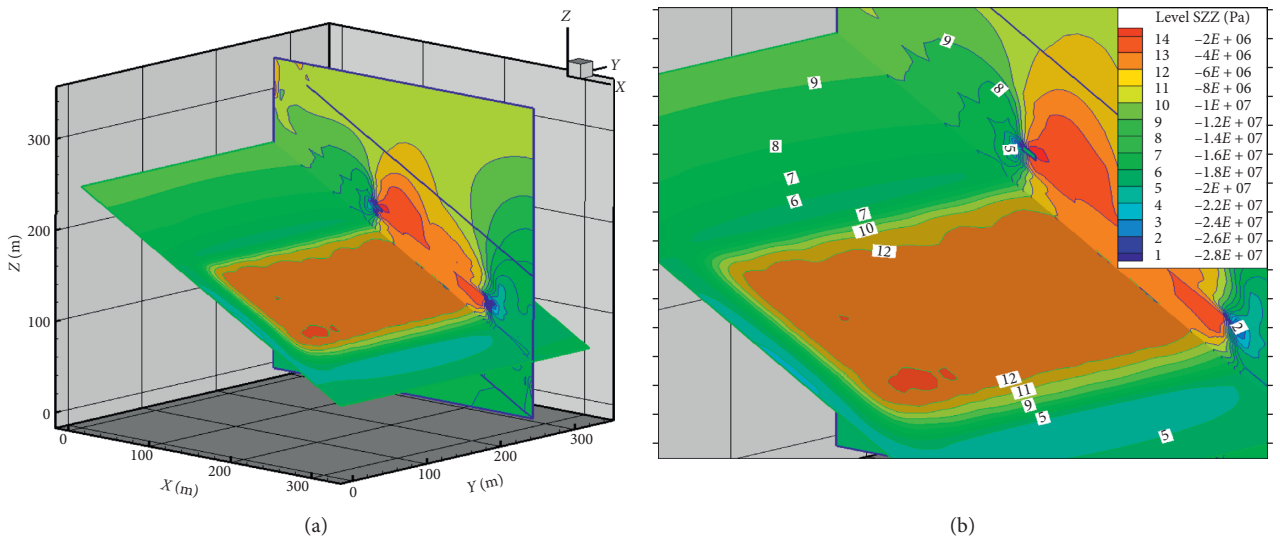

Figure 16: Vertical stress distribution in the 12124 working face after the completion of mining in the 12125 working face. (a) 3D section of the mining area (along the working face dip). (b) An enlarged image of part of the working face.

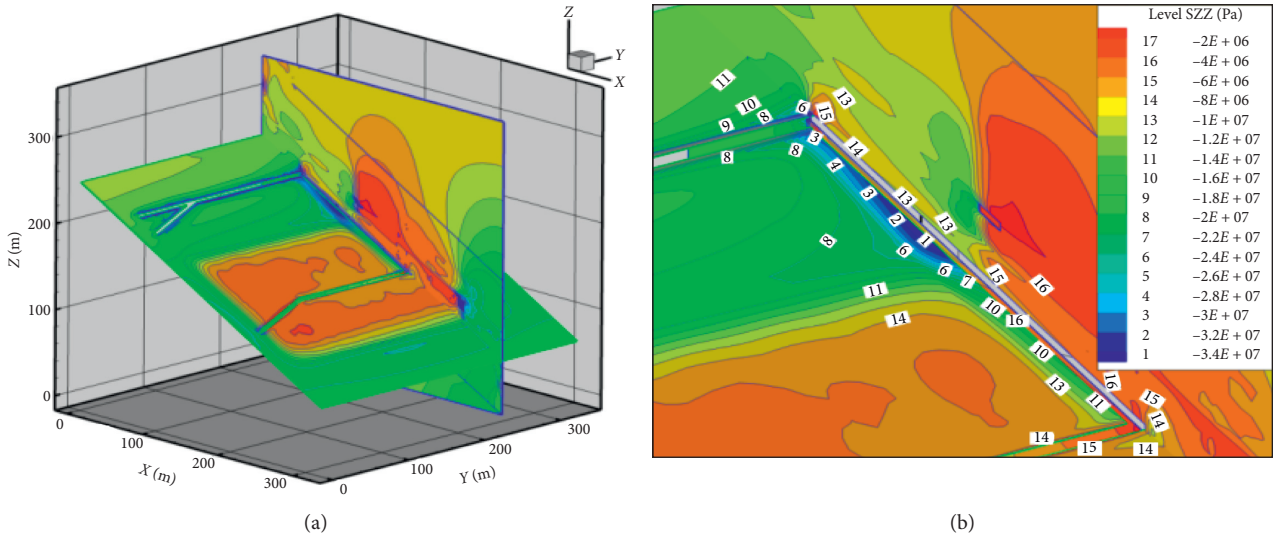

Figure 17: Vertical stress distribution in the 12124 working face. (a) 3D section of the mining area (along the working face dip). (b) An enlarged image of part of the working face.

(3) Chemical grouting can effectively improve the mechanical strength of damaged coal. However, the liquid flow in cracks/fissures in coal is uncontrollable, and liquid often overflows along the MCWS, increasing grouting consumption and cost. Water injection into the coal wall is an inexpensive and convenient measure that can improve the cohesion and friction angle of coal, enhancing its shear strength. Conventional guard gears, such as wood and bamboo anchors, increase the cohesion of coal and MCWS but lack ductility and strength. Flexible coir rope combines good ductility with high tensile and shear strength values and can accommodate large-scale coal wall deformation. It can even suspend the slip body if element failure occurs, provided the slip body satisfies the frictional sliding condition. Therefore, a new flexible protection technique called "coir rope plus grouting" was adopted here, and it greatly improved the antisliding capacity of the slip body [40]. The construction diagram is shown in Figure 18. The angle between the coir rope and MCWS should be large enough during construction when the coir rope is imposed above the upper coal and the oblique hole is drilled. The programs and optimal parameters of the flexible support technique for various geological conditions are listed in Table 1.

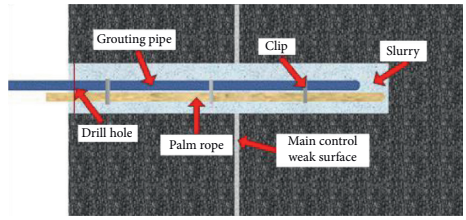

Figure 18: Construction diagram of the "coir rope plus grouting" flexible protection technique.

Table 1: Programs and parameters of the flexible support technique [40].

Program	Bore diameter, cm	Hole depth, m	Angle, °	Spacing, m	Distance from the floor, m	Coir rope diameter, cm
Normal region	42	8	40	4	2.6	25
Tectonic region	28	6	50 ± 2	2	1.8	15
Complex region	76	30	3-4	4	2	30

(4) A double metal mesh should be used to reinforce the support. Given the poor roof integrity in the 12124 working face, a universal beam and double metal mesh are recommended to help the hydraulic support bear the crushed roof load. The metal mesh length should be long enough to ensure that it is normal to the front of the hydraulic support (see Figure 19(a)). To reinforce the hydraulic support, the side guard plate length should be increased to 3 m from the original 1.5 m, and the normal load should be applied to the full section of the coal wall (see Figure 19(b)). As recommended, universal beams were horizontally bound by iron wires above the metal mesh in front of the hydraulic support. Wires and universal beams were kept close to the coal wall by guard plates to provide more support from the guard plates (see Figure 19(c)). During mining, the guard plates were withdrawn, and the metal mesh was tied up around the pillar by iron wires. The metal mesh was released from the pillar, and guard plates were laid against the coal wall after mining ended. The metal mesh and universal beams were covered at the top of the support after support shifting, which could effectively prevent fractured roof collapse (see Figure 19(d)).

(5) The loaded supports should be removed from the bottom to top, and the roof should be approached, while closely following the mining machine. The support-removal process should follow the "decline lightly and pull fast" principle to promptly support the immediately exposed roof and to reduce the spalling roof's collapse so that a roof at a high level will not spall and slide down, knocking down the support. Antisliding jacks should be arranged between every three roof beams and bases and every six four-bar linkages, as shown in Figure 20.

(6) Based on the mechanical model of Section 5 and the geological conditions and support technical parameters of the 12124 working face, the following values were determined: $\alpha = 38^{\circ}$, $\chi = 25\,\text{kN/m3}$, $H = 3.8\text{m}$, $L_s = 5\text{m}$, $B = 1.5\text{m}$, $h = 2.4\text{m}$, $\mu_1' = \mu_2' = 0.37$, $G_s = 240\,\text{kN}$, and $\varpi = 7^{\circ}$; the critical forces between the supports under the dumping state and sliding state were calculated to be -134.4 kN and 89.4 kN. The minimum force between the side jack's support should not exceed 89.4 kN to prevent support instability.

6.3. Performance of Integrated Control Measurements. The abovementioned integrated control measurements were employed in the surrounding rock in the 12124 working face. The support work resistance in the mining area of 125–171 m was monitored, and some of the results are plotted in Figure 21. As observed, as mining proceeded, the lower part of the support always exhibited the largest work resistance, and the upper part exhibited the smallest one. Compared with Figure 4, the work resistance in all parts had the same variation pattern and fluctuated within a small range of 2200–4000 kN. This implies that the roof remained stable after the integrated control scheme was applied. No-load conditions were not observed in the support, which had good stability. Additionally, no large-scale spalling or roof collapse occurred in the working face. The integrated control

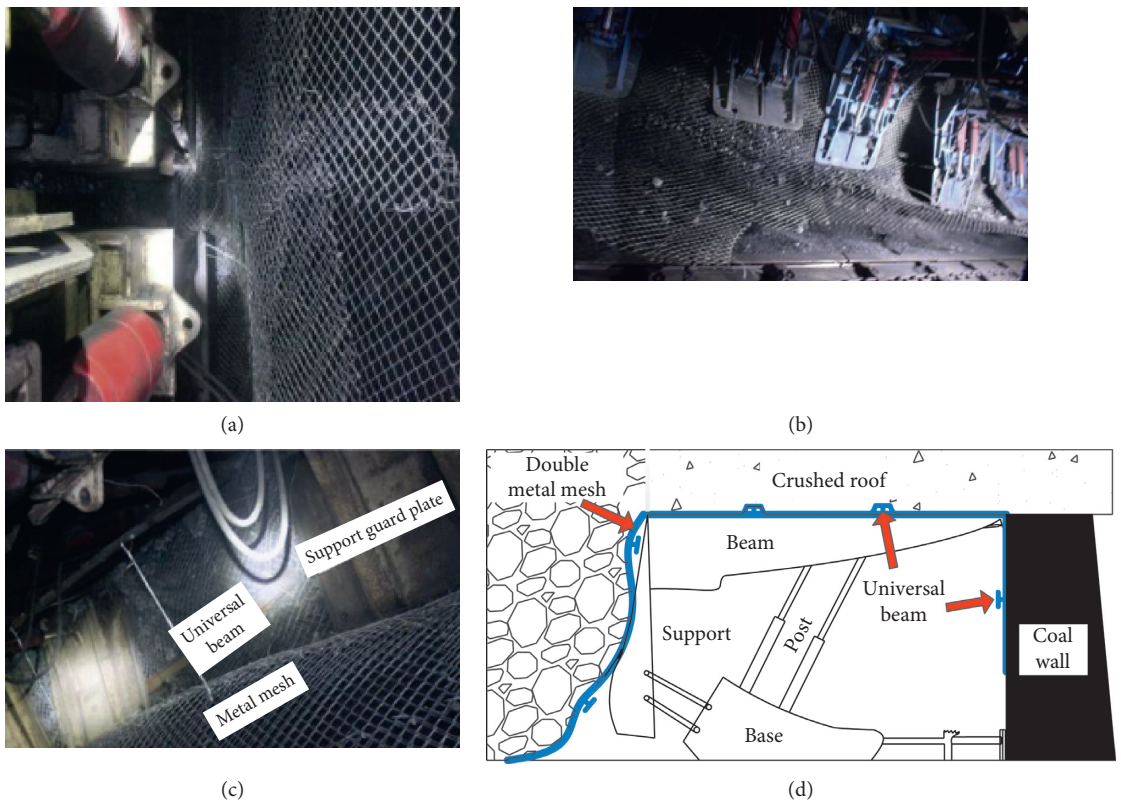

Figure 19: The support enhancement program for the coal wall and roof. (a) Double metal mesh on support. (b) Enlarged guard plate. (c) Support with guard plate, metal mesh, and universal beam. (d) Section of coalface.

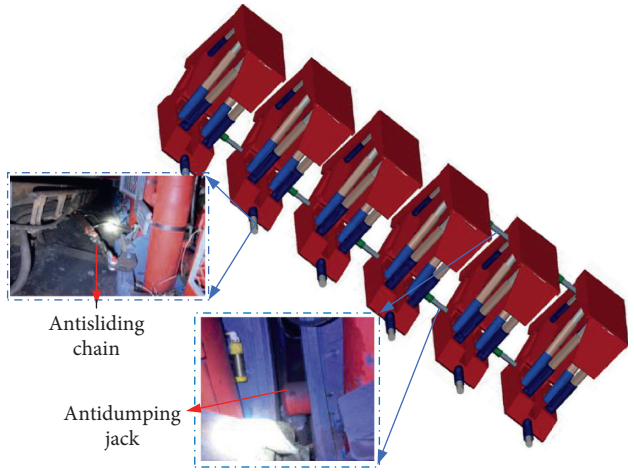

Figure 20: Antisliding and antidumping measures for hydraulic supports.

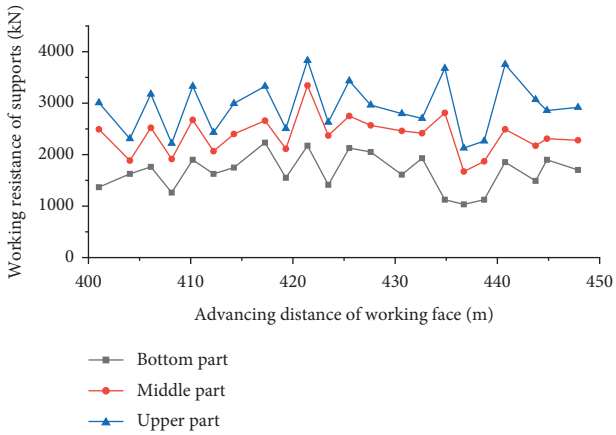

Figure 21: Monitoring results of the support work resistance in the working face.

measurements effectively prevented the occurrence of hazard chains, which ensured safe and efficient mining.

7. Conclusions

(1) The characteristics of a hazard chain's stratum behavior in an SDCS working face with a large cutting height were obtained via field monitoring. Numerous MCWSs were randomly distributed in the coal wall's plastic failure zone, which was verified by the proposed 3D physical model of the coal wall. The mechanical analysis showed that the rib spalling scales in the same working face were controlled by the shape, size, and friction angle of the triangular prism element. Shear failure and frictional sliding criteria for the coal wall elements were proposed. Single-factor sensitivity analysis revealed the following sensitivities of different factors influencing the shear failure of the coal wall element: the roof load (6.33), dip of the panel (−5.03), friction angle of the coal (−3.24), cohesion of the coal (−3.02), and sidewall protecting force (−0.087). Additionally, the sensitivities of the factors influencing slip body frictional sliding were as follows: the MCWS cohesion (−0.293), roof load (0.213), and MCWS cohesion (−0.079).

(2) The wall spalling in soft coal seams usually led to continual roof collapse, causing the adjacent supports in the immediate roof at a high level to fracture and slide down to the upper exit channel of the support below and changing the support load-bearing characteristics. The pressure exerted on the support bore changed from a stable static load to the sliding roof's dynamic load.

(3) The mechanical model of the support under the sliding roof condition, which considered the downward mining angle of the support, was established. The expressions for deriving the critical force between supports provided by jacks on guard plates under the conditions of support dumping and sliding critical limit states were proposed. The critical force between the supports depended on the friction coefficient between the roof and floor and the support, immediate roof thickness, coal dip, length of the support, and downward mining angle.

(4) Based on the mechanism of chain disasters in the 11224 working face, integrated preventive measures were proposed and tested. The work resistance of the support was raised by one-third of its original level, while water injection into the coal wall and the "coir rope plus grouting" flexible protection technique were jointly utilized to prevent the weak coal wall from failing and sliding. To prevent the immediate roof from falling, a double metal mesh was laid above the supports and in front of the coal wall. The loaded supports were removed from the bottom to top, and the roof was approached, while closely following the mining machine. Antidumping and antisliding jacks were set up on the roof beam and base of support. It was ensured that the force between supports provided by the jacks on the guard plates was no less than 86.3 kN to avert the dumping and sliding of the supports. The proposed integrated control measurements of "rib spalling - roof collapse - support instability" disasters in the working face of an SDCS with a large cutting height proved to have good application value in the mining site and ensured safe and efficient mining.

Data Availability

The data used to support the findings of this study are available from the corresponding author upon request.

Conflicts of Interest

The authors declare that they have no conflicts of interest.

Authors' Contributions

All the authors contributed to publishing this paper. Shuai Liu prepared and edited the manuscript. Ke Yang and Chunan Tang participated in the data processing during the research process.

Acknowledgments

This research was funded by the the Institute of Energy, Hefei Comprehensive National Science Center under Grant no.19KZS203, National Natural Science Foundation of China (no.51634007), and University Synergy Innovation Program of Anhui Province (Grant no.GXXT-2019-029)

References

[1] Y. P. Wu, D. F. Yun, P. S. Xie, H. W. Wang, D. Lang, and B. S. Hu, "Progress, practice and scientific issues in steeply dipping coal seams fully-mechanized mining," *Journal China Coal Society*, vol. 45, pp. 24–34, 2020.

[2] J. Guo, L. Ma, Y. Wang, and F. Wang, "Hanging wall pressure relief mechanism of horizontal section top-coal caving face and its application-A case study of the urumqi Coalfield," *China. Energies*, vol. 10, no. 9, p. 1371, 2017.

[3] P. Xie, Y. Luo, Y. Wu, X. Gao, S. Luo, and Y. Zeng, "Roof deformation associated with mining of two panels in steeply dipping coal seam using subsurface subsidence prediction model and physical simulation experiment," *Mining, Metallurgy & Exploration*, vol. 37, no. 2, pp. 581–591, 2020.

[4] H. Tu, S. Tu, Y. Yuan, F. Wang, and Q. Bai, "Present situation of fully mechanized mining technology for steeply inclined coal seams in China," *Arabian Journal of Geosciences*, vol. 8, no. 7, pp. 4485–4494, 2015.

[5] P. S. Xie and Y. P. Wu, "Deformation and failure mechanisms and support structure technologies for goaf-side entries in steep multiple seam mining disturbances," *Archives of Mining Sciences*, vol. 64, pp. 561–574, 2019.

[6] F. H. Ma, L. Sun, and D. Li, "Numerical simulation analysis of covering rock strata as mining steep-inclined coal seam under fault movement," *Trans Nonferrous Met Soc China*, vol. 21, pp. 556–561, 2011.

[7] Y. P. Wu, K. Z. Liu, D. F. Yun, P. S. Xie, and H. W. Wang, "Research progress on the safe and efficient mining technology of steeply dipping seam," *Journal China Coal Society*, vol. 39, pp. 1611–1618, 2014.

[8] Q. Jia, W. Li, and D. Che, "A triangulated irregular network constrained ordinary kriging method for three-dimensional modeling of faulted geological surfaces," *IEEE ACCESS*, vol. 8, pp. 85179–85189, 2020.

[9] X. Ding, W. Zhou, X. Lu et al., "Distribution characteristics of fragments size and optimization of blasting parameters under blasting impact load in open-pit mine," *IEEE ACCESS*, vol. 7, pp. 137501–137516, 2019.

[10] D. Che and Q. Jia, "Three-dimensional geological modeling of coal seams using weighted Kriging method and multi-source data," *IEEE ACCESS*, vol. 7, pp. 118037–118045, 2019.

[11] X. Chi, K. Yang, and Q. Fu, "Analysis of regenerated roof and instability support control countermeasures in a steeply dipping working face," *Energy Exploration & Exploitation*, vol. 38, no. 4, pp. 1082–1098, 2020.

[12] S. He, D. Song, Z. Li et al., "Precursor of spatio-temporal evolution law of MS and AE activities for rock burst warning in steeply inclined and extremely thick coal seams under caving mining conditions," *Rock Mechanics and Rock Engineering*, vol. 52, no. 7, pp. 2415–2435, 2019.

[13] K. Yang, S. Liu, C. A. Tang, Z. Wei, and X. L. Chi, "Mechanism and prevention of coal seam rib spalling in remote protected layer across coal group," *Journal China Coal Society*, vol. 44, pp. 2611–2621, 2019.

[14] X. Hao, W. Du, Y. Zhao et al., "Dynamic tensile behaviour and crack propagation of coal under coupled static-dynamic loading," *International Journal of Mining Science and Technology*, vol. 30, no. 5, pp. 659–668, 2020.

[15] Y. P. Wu, B. S. Hu, P. S. Xie, S. H. Li, and J. Y. Huangpu, "Impact damage of flying gangue in steeply dipping seams and its control," *Journal China Coal Society*, vol. 43, pp. 2694–2702, 2018.

[16] X. Li, Z. Wang, and J. Zhang, "Stability of roof structure and its control in steeply inclined coal seams," *International Journal of Mining Science and Technology*, vol. 27, no. 2, pp. 359–364, 2017.

[17] H. Zhang and Y. P. Wu, "Coal wall caving mechanism of longwall large mining height stope in steeply dipping coal seams," *International Journal of Mining Science and Technology*, vol. 36, pp. 331–337, 2019.

[18] H. W. Wang, Y. P. Wu, P. S. Xie, S. H. Luo, K. Z. Liu, and M. F. Liu, "Coal rib stability effect of mining-thickness with large mining height of working face in steeply inclined seams," *International Journal of Mining Science and Technology*, vol. 35, pp. 64–70, 2018.

[19] P. J. Yang, C. Y. Liu, and F. F. Wu, "Breakage and falling of a high coal wall in a thick mined seam," *Journal of China University of Mining and Technology*, vol. 41, pp. 371–377, 2012.

[20] Y. P. Wu, D. Lang, and P. S. Xie, "Mechanism of disaster due to rib spalling at fully-mechanized top coal caving face in soft steeply dipping seam," *Journal China Coal Soc*, vol. 41, pp. 1878–1884, 2016.

[21] H. W. Wang, Y. P. Wu, J. Q. Jiao, S. H. Luo, K. Z. Liu, and P. S. Xie, "Study on effect of dip angle on coal wall spalling of working face with great mining height in steeply inclined coal seam," *International Journal of Mining Science and Technology*, vol. 36, pp. 728–735, 2019.

[22] S. H. Luo, Y. P. Wu, P. S. Xie, H. W. Wang, and H. Zhang, "Mechanical analysis of support stability in longwall mining of steeply dipping seam," *Journal of China Coal Society*, vol. 44, pp. 2664–2672, 2019.

[23] T. Zhao, Z. Zhang, Y. Yin, Y. Tan, and X. Liu, "Ground control in mining steeply dipping coal seams by backfilling with waste rock," *Journal of the Southern African Institute of Mining and Metallurgy*, vol. 118, no. 1, pp. 15–26, 2018.

[24] D. Yun, Z. Liu, W. Cheng, Z. Fan, D. Wang, and Y. Zhang, "Monitoring strata behavior due to multi-slicing top coal caving longwall mining in steeply dipping extra thick coal seam," *International Journal of Mining Science and Technology*, vol. 27, no. 1, pp. 179–184, 2017.

[25] Y. P. Wu, B. S. Hu, P. S. Xie, and H. W. Wang, "Development and application of support and control system for simulating test based on the coupling principle of support-surrounding rocks," *Chinese Journal of Rock Mechanics and Engineering*, vol. 37, pp. 374–382, 2018.

[26] Y. P. Wu, J. Y. Huangpu, S. H. Luo, Y. Q. Wu, B. H. Liu, and W. H. Liu, "Overburden movement and roof failure characteristics in steeply dipping and close distance coal seam mining," *Journal of Xi'an University of Science and Technology*, vol. 40, pp. 1–10, 2020.

[27] S. H. Luo, Y. P. Wu, P. S. Xie, H. W. Wang, B. H. Liu, and A. Li, "Load and instability characteristics of support in large mining height fully-mechanized face in steeply dipping seam," *Journal China Coal Society*, vol. 43, pp. 3320–3328, 2018.

[28] P. S. Xie, Y. P. Wu, H. W. Wang, X. C. Gao, S. G. Ren, and Y. F. Zeng, "Stability analysis of incline masonry structure and support around longwall mining face area in steeply dipping seam," *Journal China Coal Society*, vol. 37, pp. 1275–1280, 2012.

[29] Y. J. Xu, G. F. Wang, and H. W. Ren, "Theory of coupling relationship between surrounding rocks and powered support," *Journal China Coal Society*, vol. 40, pp. 2528–2533, 2015.

[30] J. A. Wang, J. W. Zhang, X. M. Gao, J. D. Wen, and Y. D. Gu, "Fracture mode and evolution of main roof stratum above fully mechanized top coal caving longwall coalface in steeply inclined thick coal seam (II): periodic fracture," *Journal China Coal Society*, vol. 40, pp. 1737–1745, 2015.

[31] Y. Yuan, S. H. Tu, F. J. Dou, and Q. Wu, "Support instability mechanism of fully mechanized top coal caving face with

steep coal seams and its control," *International Journal of Mining Science and Technology*, vol. 25, pp. 430–434, 2008.

[32] H. Alehossein and B. A. Poulsen, "Stress analysis of longwall top coal caving," *International Journal of Rock Mechanics and Mining Sciences*, vol. 47, no. 1, pp. 30–41, 2010.

[33] N. Bilim and İ. Özkan, "Determination of the effect of roof pressure on coal hardness and excavation productivity: an example from a Çayırhan lignite mine, Ankara, Central Turkey," *International Journal of Coal Geology*, vol. 75, no. 2, pp. 113–118, 2008.

[34] J. C. Wang, "Mechanism of the rib spalling and the controlling in the very soft coal seam," *Journal China Coal Society*, vol. 32, pp. 785–788, 2007.

[35] X. W. Yin, S. H. Yan, and N. An, "Characters of the rib spalling in fully mechanized caving face with great mining height," *International Journal of Mining Science and Technology*, vol. 25, pp. 222–225, 2008.

[36] Y. Ning, "Mechanism and control technique of the rib spalling in fully mechanized mining face with great mining height," *Journal China Coal Society*, vol. 34, pp. 50–52, 2009.

[37] Y. Tai, H. Xia, and T. Kuang, "Failure characteristics and control technology for large-section chamber in compound coal seams-A case study in Tashan Coal Mine," *Energy Science & Engineering*, vol. 8, no. 4, pp. 1353–1369, 2020.

[38] G. F. Wang, Y. J. Xu, and D. Y. Li, "Analysis on supporting principle and its application of powered support in large inclined fully mechanized face based on balance of rigid and flexible combined overturning moment," *Chinese Journal of Rock Mechanics and Engineering*, vol. 37, pp. 4125–4132, 2018.

[39] X. Hao, Y. Wei, K. Yang et al., "Anisotropy of crack initiation strength and damage strength of coal reservoirs," *Petroleum Exploration and Development*, vol. 48, no. 1, pp. 243–255, 2021.

[40] S. L. Yang and D. Z. Kong, "Flexible reinforcement mechanism and its application in the control of spalling at large mining height coal face," *Journal China Coal Society*, vol. 40, pp. 1361–1367, 2015.